Applied Energy 287 (2021) 116588

Contents lists available at ScienceDirect

Applied Energy

journal homepage: www.elsevier.com/locate/apenergy

A methodology for architecture agnostic and time flexible representations of wave energy converter performance

Bryson Robertson [a,b,*], Helen Bailey [d], Matthew Leary [a], Bradley Buckham [c]

[a] Oregon State University, Corvallis, USA
[b] Pacific Northwest National Laboratory, Portland, USA
[c] University of Victoria, Victoria, Canada
[d] Simon Fraser University, Vancouver, Canada

HIGHLIGHTS

- New tractable methods developed to allow rapid determination of wave energy production at improved temporal resolution.
- Presentation of performance matrices for five different wave energy converter architectures; all developed using a consistent and validated numerical model.
- Development of a generic wave energy converter performance model to quantify performance; including rated power and cut-in levels.
- The generic WEC performance model has average R^2 of 0.93 and less than 9% variation in annual energy production when compared against specific WEC architectures.
- New methodology defined to temporal up-sample wave conditions to increase ability to predict sub-hourly WEC performance.

ARTICLE INFO

Keywords:
Wave energy converter
Power production
Generic model
Temporal sampling
Resource assessment
Wave spectra

ABSTRACT

The growth of the wave energy sector is contingent on the ability for stakeholders, particularly electrical utilities, to rapidly predict the production from wave energy converters (WECs). Current methodologies require extensive knowledge of metocean conditions, *a priori* determination of WEC architecture, and highly-specific physical and numerical tools. Additionally, the lack of a consistent robust method to up-sample the hourly temporal resolution of traditional wave buoys and/or numerical wave propagation models limits the implementation of wave energy technologies in Integrated Resource Planning (IRP) by utilities. These two knowledge gaps create a significant barrier for broad adoption of wave energy. This novel research provides an overview of a waves-to-wire method to quantify WEC performance, across a wide variety of technology architectures, to develop an empirically driven and easily applicable generic model of WEC performance. The generic WEC performance model ultimately shows an average co-efficient of determination (R^2) of 0.93 and less than 9% variation in annual energy production when compared against five significantly different WEC architectures. The temporal up-sampling methodology is shown to generate wave resource and WEC performance data at a resolution suitable for an IRP process, creates a realistic representation of wave condition variability on short-time frames, and does not artificially perturb the available energy on an annual basis.

1. Introduction

The growth and continued development of the wave energy sector is contingent on the ability for stakeholders to rapidly assess and predict the future production from wave energy converters (WECs). A wealth of information is available in both publicly literature and academic journals concerning different methodologies and associated results derived from deploying a specific WEC architecture at a particular location. Many of these results require extensive knowledge of metocean conditions, a broad understanding of marine energy-specific terminology, and highly-specific tools (physical and numerical) by the stakeholder prior to application. This creates a significant barrier for broad adoption of wave energy. There is a significant and immediate need for easily implementable methods and representations of WEC performance,

* Corresponding author at: Oregon State University, Corvallis, USA.
E-mail address: bryson.robertson@oregonstate.edu (B. Robertson).

https://doi.org/10.1016/j.apenergy.2021.116588
Received 16 November 2020; Received in revised form 24 January 2021; Accepted 28 January 2021
Available online 9 February 2021

based on publicly available data, in order to facilitate a broader adoption of wave energy by stakeholders and investors (electrical utilities, energy policy makers, aquaculture facilities, etc.)

The most popular methods to predict the power and annual energy production from a WEC follows guidelines set forth by International Electrotechnical Commission TC-114 committees. The IEC TC-114 is convened to facilitate uniform methods of predicting production from wave energy converters. Technical Standard 62600-101 '*Wave resource assessment and characterization*' recommends that wave resources are characterized by a bi-variate histogram of significant wave height (H_s in 0.5 m bins) and energy period (T_e in 1 s bins), based either on direct measurements of wave conditions (via buoys, ADCP's, etc.) or validated numerical wave propagation model outputs [1]. The assessment of wave energy resources is paramount in the development of any future WEC project. As such, there is a wealth of valuable on-going research to continually develop improved methodologies for resource assessments for specific devices or arrays; these include works by Lenee-Bluhm et al. [2], Robertson et al. [3], Lopez-Ruiz et al. [4], and Luzko et al. [5]. Additionally, there has been significant efforts to quantify wave resources in specific locations due to local wave transformations and dynamics. A non-exhaustive list includes wave resources in Northern Europe [6–8], North Africa [9], Uruguay [10] Australia [11,12], South Africa [13], Canada [14,15] amongst others.

Independently, the IEC Technical Standard 62600-100 '*Electricity producing wave energy converters – Power performance assessment*' recommends that the mean power produced from a WEC is mapped against the same bivariate histogram/matrix (known as a 'WEC performance matrix'), based on experiential testing and hydrodynamic modelling. In order to determine the final production from a specific WEC in a specific location, the time-series of H_s and T_e is used to identify the appropriate power performance from the WEC performance matrix and associated power production. This suggested IEC methodology provides a robust methodology if the technology, or WEC architecture, is known *a priori*. Additionally, leaves project developers and utilities reliant on WEC developers executing the IEC TS 62600-100 (which can take up to a year) and publicly releasing that information.

For many stakeholders, the technology choice is, at best, still unknown or, at worst, irrelevant until initial resource screen and supply stack analysis completed. The commercial trajectories of many WEC architectures are still too uncertain, so fulfilling this *a priori* requirement represents a significant effort/understanding barrier. As such, planning for electricity generating resource futures tend to focus on more identifiable and easily characterized resources, such as wind and solar resources, or near-commercial innovation, such as floating offshore wind or enhanced geothermal systems [16,17].

For competing renewable energy generators, like wind or solar, agnostic representations of technology performance are utilized to provide generic representation of performance and paved the way for larger scale adoption. For the wind sector, as shown in Fig. 1, the performance of a wind turbine can be determined by wind speed [18]. The performance is divided into three regions: a below cut-in wind speed region, a production region, and a static rated power region (independent of wind speed). Beyond the rated power region, there is a cut-out speed not presented in Fig. 1.

For wave energy to be considered in-line with the suite of mentioned renewables, a similar methodology to create technology-agnostic and time-flexible representations of WEC power production, based on publicly available data is required. This is the objective of this paper.

In order to overcome this knowledge gap, many studies approximate performance by assuming a single-body or two-body heaving converter producing power in a single degree-of-freedom [1920], reproducing models of specific WEC architectures [2122], or providing a wholistic review of all current or historical devices [2324]. Parkinson et al. [25] generated a generic performance matrix by assuming WEC power production is proportional to raw wave resources and a proportionality constant was determined to maintain a 30–35% WEC capacity factor.

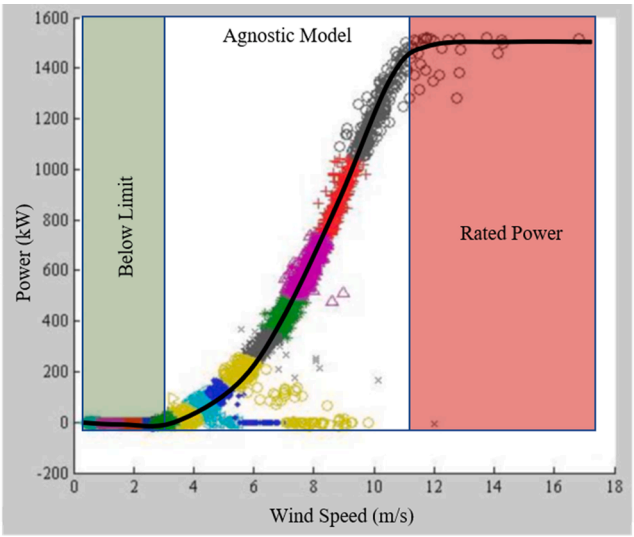

Fig. 1. Generic wind turbine performance curve (Colours represent multiple turbines in different wind regimes,).
adapted from [18]

Robertson et al. [26] used five specific WEC performance matrices from [27], divided by their individual characteristic widths (device width perpendicular to dominant wave direction), averaged and assumed a 20 m characteristic width to create a generic performance matrix. Xu et al. [28] averaged the power outputs from four WEC architectures, in the frequency-domain, to create a WEC performance estimate by frequency-domain filtering the naturally occurring wave power. Despite these continued efforts, there remains a lack of an easily implemented model that represents the non-linear dependencies of WEC power performance on significant wave height and energy period, the ability to capture power from the full six degrees of freedom, and then applies a realistic rated power capacity.

This research utilizes a database of WEC performance data developed through a consistent numerical methodology applied to a wide variety of technology architectures to develop an empirically driven and easily applicable architecture-agnostic model of WEC performance. This model is the wave energy equivalent of the standard wind turbine performance curve seen in Fig. 1. This model will provide the opportunity for project developers to rapidly scale WEC performance (across significant wave height and energy period bins, and in the absence of any decision on specific WEC architecture) to determine 'optimal' capacities and associated generation. The final 'optimal' model output can then be utilized to inform the project-specific WEC technology architecture. The relative performance and associated uncertainty of the new generic model will be analyzed against standard electrical utility performance metrics to both understand the implications of this new approach and help facilitate broader adoption of wave energy within this important stakeholder group

This paper is structured as follows: Section 2 introduces the wave energy converter architectures, physical dimensions and differing power-take-off (PTO) systems, while Section 3 reviews the consistent hydrodynamic numerical modelling and validation processes. Section 4 details the development of the generic WEC model and the inherent simplifying assumptions. Section 5 provides a methodological overview of developing time-flexible WEC power performance estimates. Section 6 reviews the implications and results of applying the developed methodologies for the case study of PacWave, USA. Section 7 and 8 provide a discussion of the results and concluding statements, respectively.

2. Wave energy converters architectures and operating principles

There are a wide variety of different WEC architectures with different operating principles, reactive systems, power-take-offs, etc. currently in development. For this work, five very different architectures are utilized to create a generic WEC representation. These include: single-body point absorber (Fig. 2a), a two-body point absorber (Fig. 2b), an oscillating surge flap (Fig. 2c), a cascading multiple body system (Fig. 2d – one body shown), and a floating oscillating water column (Fig. 2e). Specific details on each system and associated modelling are provided below. As per the technical specifications by the International Electrotechnical Commission TC-114, all performance characteristics are referenced against the significant wave height (H_s) and the energy period (T_e). The wave calculations required to derive these parameters are included in Section 5.

2.1. One body point absorber (1BPA)

One-body point absorbers consist of a singular floating body at the surface and a PTO connected to the seabed, as illustrated in Fig. 2a. The surface float moves in response to wave excitation, and the PTO harnesses the relative motion between the surface float and the seabed to extract mechanical power. The hydrodynamic forces in the system are predominantly dependent on the surface float. Generally, for point absorbers, wave energy is converted through the float's heave motion, however pitching point absorbers do exist [29].

SeaWood Designs' SurfPower WEC is an example of a single-body point absorber WEC, a model of which is shown in Fig. 2a. The SurfPower device consists of a buoyant pontoon that reacts against a sea-bed mounted hydraulic cylinder. The pontoon in the design is 24 m long, 7 m wide and 1 m in depth. The pontoon is free in five degrees of motion, while yaw is maintained via a proprietary control system. The cylinder has the ability to rotate around a fixed point, and as the pontoon moves, the cylinder expands and contracts. Energy extraction only occurs on the cylinder's upstroke, from which the pressurized fluid is transported to shore to generate electricity. A characteristic performance matrix of a numerical model of the SurfPower WEC is shown in Fig. 3 [30].

2.2. Two-body point absorber (2BPA)

Two-body point absorbers' energy conversion is due to the relative motion between two bodies: an active surface buoy, which extracts energy, and a reacting body, which passively adds to the desired inertia of the system. Two-body point absorber designs have a variety of surface buoys, reacting body shapes, mooring designs, and PTO strategies. The reacting body may be a streamlined body or a heave plate [31]. PTOs may be hydraulic (as discussed in Section 2.1), pneumatic (kinetic energy is transformed into potential energy of compressed air), or mechanical. Moorings systems range widely from single- to multi-cable, and they may follow a catenary or taut design system [32].

Examples of two-body point absorbers include the WaveBob, a model of which is shown in Fig. 2b, Ocean Power Technologies PowerBuoy, the AquaBuoy of Finerva Renewables [33], and the University of Washington's Applied Physics Laboratories miniWEC [34]. The University of Victoria built a 1:20 scaled two-body point absorber system similar to the WaveBob; consisting of a circular cylinder float with a full-scale diameter of 15 m and a streamlined 39 m spar buoy with a ballast tank [31,35,36]. For this device, a passive viscous damping PTO is utilized between the two bodies, from which the relative motion between them generates electricity. A performance matrix is shown in Fig. 4 [37].

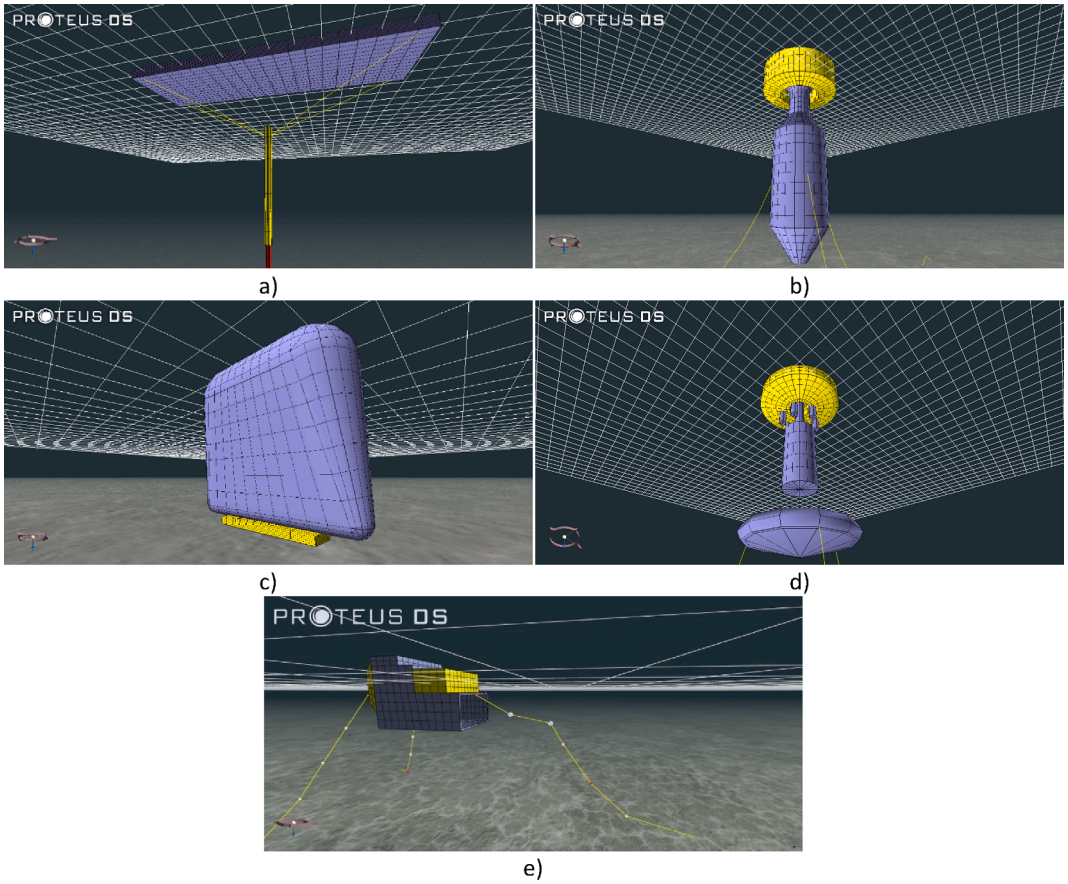

Fig. 2. WEC architectures utilized to generate generic representation.

P [W]	Wave Energy Period [s]												
Significant Wave Height [m]	5.50	6.50	7.50	8.50	9.50	10.50	11.50	12.50	13.50	14.50	15.50	16.50	17.50
0.25													
0.75			19400	11000	10900	12100	7990						
1.25		58600	85200	83000	94000	85500	69300						
1.75		147000	164000	167000	174000	156000	141000	139000					
2.25		209000	209000	235000	233000	213000	205000	196000	179000				
2.75		298000	310000	313000	308000	271000	236000	233000	216000	218000			
3.25			379000	364000	359000	335000	315000	295000	265000	265000			
3.75			435000	431000	420000	401000	368000	366000	317000	313000			
4.25				507000	473000	445000	435000	388000	376000	356000			
4.75				583000	564000	492000	482000	445000	414000	380000			
5.25					596000	553000	527000	479000	447000	410000			
5.75					625000	588000	545000	526000	479000	457000	417000		
6.25						626000	555000	558000	504000	461000	443000		
6.75						664000	601000	585000	529000	501000			
7.25													
7.75													

Fig. 3. Single-Body Point Absorber Performance Matrix.

P [W]	Wave Energy Period [s]												
Significant Wave Height [m]	5.50	6.50	7.50	8.50	9.50	10.50	11.50	12.50	13.50	14.50	15.50	16.50	17.50
0.25	696	1088	1334	1222	958	737	599	476	340	328	261	208	172
0.75	6477	10015	11428	11770	9555	6547	5781	4291	2763	2994	2480	1967	1491
1.25	16998	25599	31110	29358	24902	20870	16346	13796	8923	9939	6002	5113	3631
1.75	33240	52668	52990	58153	45288	32189	28977	22427	19632	18071	12237	11711	8333
2.25		84574	82820	99583	79710	58032	46870	40898	36048	26569	20147	14929	14583
2.75		116455	103882	127590	121768	97884	58441	52472	46319	38176	34154	24195	19660
3.25		155668	137440	168119	162732	128409	86810	76113	61458	56755	47213	40419	29582
3.75		214002	195510	190137	192015	166560	142173	110692	72417	71752	71609	53110	37157
4.25			229262	235332	255156	216426	178936	146987	127803	98797	71792	50702	49058
4.75				308900	253597	240510	218507	142699	145985	109292	94234	92561	66746
5.25					368152	321780	271532	212399	169601	151130	103961	93083	78872
5.75						336041	246740	251074	180069	143292	150160	105231	84759
6.25						394096	321218	282912	259631	202792	149217	99802	106078
6.75						349609	356687	300026	253526	228600	162578	120928	144773
7.25						476031	465555	286671	259860	235884	179791	153422	132911
7.75						464001	378678	418194	291563	285077	230664	170593	142990

Fig. 4. Two-Body Point Absorber Performance Matrix.

2.3. Oscillating surge flap (Flap)

Oscillating surge flap WEC (OSWEC) devices consist of a flap attached to a rigid base, where the flap is constrained to rotate in pitch alone (about the base through a rigid hinge) [38]. OSWECs are typically mounted to the seabed; however, some OSWEC technologies are designed to float on or near the sea surface.

Commercial OSWECs include the Oyster WEC by Aquamarine Power [39], the WaveRoller installed in Portugal [40], and Resolute Marine Energy's OSWEC [41], the Floating Oscillating Wave Energy Converter (FOSWEC) developed by researchers from the National Renewable Energy Laboratory and Sandia National Laboratory [42]. A numerical model of an OSWEC based on Resolute Marine Energy's design is shown in Fig. 2c; the WEC has a flap height of 8.8 m and is modeled to operate in 8 m depth, allowing the device to pierce the surface when vertical. The edges of the flap are curved in order to reduce viscous drag forces and the appendage moves in pitch according to wave energy forcing. This motion forces a hydraulic cylinder to pressurize seawater, which is then pumped to shore and may be utilized for a wide range of energy purposes. A performance matrix characterizing power generation for the modeled OSWEC device is shown in Fig. 5.

2.4. Cascading multiple buoy (CMB)

The cascading multiple buoy WEC concept utilizes multiple of the aforementioned WEC designs to facilitate the transfer of wave energy. An example of a cascading multiple buoy WEC is Accumulated Ocean Energy (AOE) Inc.'s WEC system, shown in Fig. 2d, which consists of three identical point absorber buoys each utilizing a pneumatic PTO system. Each point absorber in the AOE system consists a float with a diameter of 10.97 m and height of 2.79 m, and a spar with a bottom mounted heave plated that is 10.97 m diameter heave plate located 18.69 m beneath the float. Additionally, there are 6 accumulator tanks which are 1.63 m tall placed radially around a spar, and a 5.08 m tall

P [W]	Wave Energy Period [s]										
Significant Wave Height [m]	7.50	8.50	9.50	10.50	11.50	12.50	13.50	14.50	15.50	16.50	17.50
0.25			1796	1601	1296						
0.75	11178	10423	11700	9243	9290	7376	5626	4749	3683		
1.25	25665	31119	22365	23939	18402	17549	15564	13440	10134	8779	
1.75		44390	38580	38826	30984	33022	31393	22614	18271	15853	
2.25		70567	59863	49201	48077	44461	40116	36770	29886	28194	21128
2.75		85178	78792	77256	72900	62942	52322	47422			
3.25			116675	89885	83898	83825	59415	56691			
3.75						112635	111077	88295			
4.25							117412	111213			
4.75								129960			

Fig. 5. OSWEC Performance Matrix.

buoyancy tank beneath the accumulator tanks having a diameter of 1.52 m. The pneumatic PTO in the AOE system compresses air from the atmosphere with hydraulic pistons and passes the pressurized fluid to the next device through the accumulator tanks. The hydraulic piston motion of each device may not synchronize, and so accumulator tanks are used control pressure by releasing the pressurized fluid to the subsequent devices once the air in the tanks exceeds that of the piston in the next unit. Once the air in the final tank has reached a final crack pressure, the pressurized fluid is released and sent to shore. This cascaded multiple buoy system strengthens the continuity of air flow by selectively pressurizing and depressurizing the air [43]. A performance matrix characterizing power generation for the cascading multiple buoy WEC is shown in Fig. 6.

2.5. Oscillating water column (OWC)

Oscillating water columns are another type of WEC featuring an internal air chamber and oscillating water column within a rigid exterior hull. Ocean waves create a pressure differential, which causes the water column to move, acting like a piston and inducing air pressure changes to drive an internal turbine. The turbine is rigidly mounted to the hull, and provides mechanical power to a generator.

Examples of oscillating water columns include the Islay LIMPET in Scotland, the Ocean Energy Buoy deployed in the United States off of Hawaii, and the Mutriku project in the Basque country. The Backward Bent Duct Buoy (BBDB), developed by Bull et al. [44], is an example of a floating oscillating water column shown in Fig. 2e. The BBDB has a 17.5 m draft, a 27 m beam, and a 35 m length. The BBDB may be visualized as two structures: the floating structure and a separate piston. The piston represents the surface elevation of the water within the air chamber. The associated relative internal pressure of the air chamber exerts a force on both bodies, which moves a drivetrain composed of a constant speed Variable Radius Turbine. Additionally, the mooring system for the BBDB consists of a 3-point catenary mooring system. Further details on the BBDB can be found in [37]. A performance matrix characterizing power generation for the floating oscillating water column is shown in Fig. 7 [5].

3. WEC numerical modelling techniques

A wealth of IEC-specification consistent WEC performance matrices are available in the published literature. However, these matrices are generally not directly comparable due to differing modelling techniques, differing levels of validation, and different sea state assumptions [23,45,46]. This section provides a review of the consistent numerical framework utilized to generate the performance matrices in Section 2. The complex modelling approach detailed below was required to output the wealth of data exploited to generate, and establish confidence, in the generic WEC model.

The hydrodynamic forces and multi-body system dynamics for each WEC architecture are device specific. As such, identification and prioritization of individual forces on each system are essential. In order to properly characterize the hydrodynamics and PTO dynamics, a wave-to-wire simulation methodology is implemented as presented by Bailey et al. [47].

The numerical modeling process, described in Fig. 8, and detailed below presents the modelling sequence, from the geometric build to time-domain modelling, necessary to achieve a robust full-wave-to-wire simulation.

3.1. Geometric build & frequency domain modelling

In order to approximate how incoming waves excites or creates a structure's dynamic response, a geometric representation of the WEC architecture is required. The most common methods to create the geometric representation is via the development of a geometric CAD model; in SOLIDWORKS or similar packages.

To resolve the WEC's response over an entire wavefield, the geometry is subsequently discretized into a series of small panels; using Rhinoceros [48] or similar meshing software. Assuming linear waves and associated superposition theory, the velocity potential of the wave field is resolved such that response amplitude operators (RAOs) and the velocity potential are found over a range of wave frequencies. This is performed by passing the discretized geometries to a frequency-domain Boundary Element Method (BEM) solver, such as WAMIT [49], NEMOH [50], or ShipMo3D [51]. The BEM model solves the velocity potential at each mesh panel, based on linear superposition of individual wave components. Following Newman [52], this is represented by:

$$\sum_{j=1}^{6}\left[-\omega\left(M_{-ij}+A_{-ij}\right)+i\omega B_{-ij}+C_{-ij}\right]\xi_j = X_i \tag{1}$$

where i and j refer to particular degrees of freedom, ω is the angular wave frequency, M_{-ij} specifies structure's inertia matrix, A_{-ij} is the added mass matrix, B_{-ij} holds the damping coefficients, and C_{-ij} contains the hydrostatic coefficients. The term ξ_j denotes the complex amplitudes of oscillatory motions in each degree of freedom, and the output X_i marks the excitation forces in each degree of freedom, denoting the Haskind relations [52].

The BEM calculations output the hydrodynamic coefficients acting on the WEC structures, that are subsequently utilized for time-domain modelling to represent the WEC architecture's forces as a function of time.

3.2. Time domain modelling

Conversion from frequency-domain BEM modelling into the time-domain enables higher order numerical schemes to better resolve interactions between waves and floating bodies; including the calculation

P [W]		Wave Energy Period [s]												
		5.50	6.50	7.50	8.50	9.50	10.50	11.50	12.50	13.50	14.50	15.50	16.50	17.50
Significant Wave Height [m]	0.25	696	1090	1330	1220	958	737	599	476	340	328	261	208	172
	0.75	6480	10000	11400	11800	9550	6550	5780	4290	2760	2990	2480	1970	1490
	1.25	17000	25600	31100	29400	24900	20900	16300	13800	8920	9940	6000	5110	3630
	1.75	33200	52700	53000	58200	45300	32200	29000	22400	19600	18100	12200	11700	8330
	2.25		84600	82800	99600	79700	58000	46900	40900	36000	26600	20100	14900	14600
	2.75		116000	104000	128000	122000	97900	58400	52500	46300	38200	34200	24200	19700
	3.25		156000	137000	168000	163000	128000	86800	76100	61500	56800	47200	40400	29600
	3.75		214000	196000	190000	192000	167000	142000	111000	72400	71800	71600	53100	37200
	4.25			229000	235000	255000	216000	179000	147000	128000	98800	71800	50700	49100
	4.75				309000	254000	241000	219000	143000	146000	109000	94200	92600	66700
	5.25					368000	322000	272000	212000	170000	151000	104000	93100	78900
	5.75						336000	247000	251000	180000	143000	150000	105000	84800
	6.25						394000	321000	283000	260000	203000	149000	99800	106000
	6.75						350000	357000	300000	254000	229000	163000	121000	145000
	7.25						476000	466000	287000	260000	236000	180000	153000	133000
	7.75						464000	379000	418000	292000	285000	231000	171000	143000

Fig. 6. Performance Matrix for the AOE WEC.

P [W]		Wave Energy Period [s]									
		5.50	6.50	7.50	8.50	9.50	10.50	11.50	12.50	13.50	14.50
Significant Wave Height [m]	0.25										
	0.75		838	3590	5700	8050	7390	7430	5680		
	1.25		3760	13800	19900	27300	28000	24600	20700		
	1.75		11000	31400	52500	57000	52700	51300	40400	34700	
	2.25		22700	57800	88200	94600	88200	85100	70000	64700	
	2.75		34200	83100	120000	128000	123000	117000	106000	84100	
	3.25			115000	158000	177000	165000	162000	129000	119000	
	3.75			152000	204000	203000	209000	182000	169000	147000	143000
	4.25				234000	253000	229000	232000	201000	181000	156000
	4.75					277000	272000	261000	227000	197000	180000
	5.25						303000	240000	252000	252000	
	5.75						296000	296000	279000		
	6.25										
	6.75										
	7.25										
	7.75										

Fig. 7. Floating Oscillating Water Column Performance Matrix.

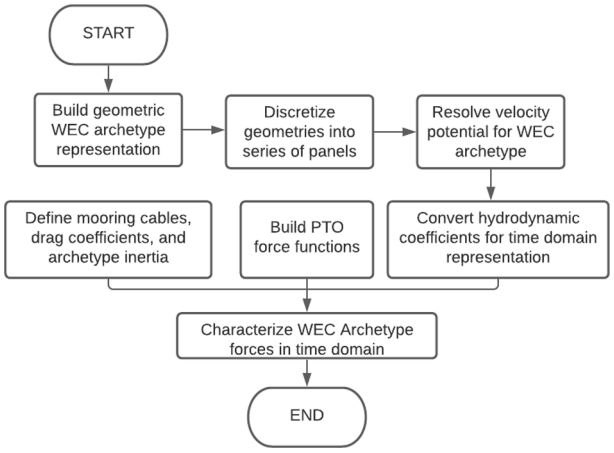

Fig. 8. Generic WEC Modeling Process.

of viscous drag and PTO forces, two inherently nonlinear processes. With the appropriate hydrodynamic forces and excitations specified, a full wave-to-wire simulation may be performed for the desired WEC. The time domain numerical model utilizes Eq. (2), which accounts for all the major forces acting on the system:

$$\left(M_{-}+A_{\infty}\right)\ddot{x}(t)=F_{exc}(t)+F_{rad}(t)+F_{pto}(t)+F_{drag}(t)+F_{B}(t)+F_{m}(t) \quad (2)$$

where M_{-} refers to the same inertia matrix as in Eq. (1), A_{∞} is the added mass at infinite frequency, $\ddot{x}(t)$ is the acceleration of the bodies, F_{exc} is the wave excitation force, F_{rad} is the radiation force containing the frequency dependent added mass and damping terms, F_{pto} is the PTO force, F_{drag} is the drag force, F_B is the buoyancy force, and F_m is the mooring force [27]. For this study, ProteusDS was utilized as the time-domain modelling platform [53]. These forces and co-efficient sources are detailed below.

3.2.1. Excitation force

The excitation force is the summation of the dynamic pressures across the body panels from incoming and diffracted waves. These forces are loaded into ProteusDS from the BEM solver, and are resolved across the wetted portion of the WEC architecture.

3.2.2. Radiation force

To calculate the radiation force, the hydrodynamic coefficients from WAMIT are calculated with a kernel function. The kernel function represents the decaying time domain response of each body to a unit impulse. From this, a convolution integral is taken with the body velocity to represent the radiation force [53].

3.2.3. Power Take-Off (PTO) force

PTO systems vary between WEC architypes and include mechanical, pneumatic, and hydraulic systems (associated dynamics are discussed in Section 2); as such, a flexible methodology to properly characterize their performance is necessary. To facilitate the varying dynamics of the PTO force, ProteusDS's Application Programming Interface (API) toolbox is utilized to facilitate custom PTO systems. PTO force functions are built in MATLAB Simulink in the form of s-functions, which are used to characterize PTO-specific quantities such as piston stroke length, fluid velocity, air pressure, etc., based on outputs from ProteusDS via a direct library link (DLL) [47].

3.2.4. Drag force

The non-linear drag force is calculated individually for each panel in ProteusDS utilizing the Morison equation to determine viscous drag, and then is summed over the WEC's surface. The drag force is calculated for each panel of the WEC architecture's discretized surface. It is proportional to the square of the relative motion between the WEC and neighboring water particles, and an architecture specific drag coefficient.

3.2.5. Inertial force

The inertial force includes both the object mass and the added mass at infinite frequency (from the BEM calculation) multiplied by acceleration as shown on the left-hand side of Eq. (2). This side of the equation demonstrates how the change in velocity of the WEC architecture results in a change in the associated forces of the system representing Newton's second law.

3.2.6. Buoyant force

The buoyant force is calculated utilizing hydrostatic coefficients C_{ij} from Eq. (1) to calculate buoyancy. For WECs with dynamic wetted surface areas, nonlinear buoyancy calculations are made by summing the hydrostatic pressure over the submerged surface of the body.

3.2.7. Mooring line tension

The mooring line tension is calculated using a cubic spline lumped mass cable model [54]. Cable material properties are specified along the cable. The cable is discretized into a set of elastic elements, for which forces from waves, neighboring elements, and structures are calculated through finite element analysis for time progression.

4. Architecture agnostic WEC representations

A key requirement for the ubiquitous uptake of wave energy in energy system planning and other emerging markets is easily applicable and WEC architecture agnostic representation. Regardless of whether planning for a grid-scale utility system or a remote isolated grid, a 2 yr. or 20 yr. timeline, or a unique non-wires opportunity, the WEC representation needs to be applicable across a wide range of wave conditions, needs to account for realistic rated power limits, and needs to be flexible to a variety of temporal characteristics.

4.1. Consistent wave conditions and normalized power output

Utilizing the presented database of WEC concepts, all developed with the same numerical processes and sea state characterizations, allows for direct comparison and the development of a generic representation. As per IEC TC-114: 101 [1], the WEC performance matrices were all designed to cover a significant wave height (H_s) variation from 0 m to 8 m, in 0.5 m bins, and an energy period (T_e) from 5 s to 18 s, in 1 s bins. While it is acknowledged that some WECs will produce power in lower than 4.5 s waves, the WEC concepts utilized in this work were focussed on utility scale generation and, hence, were larger and had higher natural periods.

Initially, all wave conditions above the deep-water breaking limit of $H_{max} \approx 0.14(1.56T_e^2)$ were removed since these wave conditions are not realistic [55]; despite their frequent appearance in published WEC performance matrices. Next, all the individual performance matrices were normalized by their respectively maximum production (so power performance was scaled from zero to one). Fig. 9 shows the normalized performance of all the WEC architectures. As shown by Xu et al.[28], the power outputs follows a similar trend when scaled by the maximum production and plotted against energy period (Fig. 9a). However, when plotting in the significant wave height and energy period space (Fig. 9b), WEC architecture dependence is noticeable. For example, the 2BPA has a small period bandwidth when compared against the BBDB.

Acknowledging these differences between device performance, this research aims to discern common features between the surfaces shown in Fig. 9b. These features could then be used to determine a single common framework, hereafter a 'generic' WEC model, that can be adjusted, in terms of a finite set of coefficients, to reasonably approximate the performance of any single device. This common framework is the wave energy parallel to the generic wind turbine performance shown earlier in Fig. 1, and the coefficients that are used to adjust the generic model are the parallels to the cut-in and cut-out speeds, the rated power, etc.

As a reminder, the gross wave energy transport (J – units: kW) in deep water depends on the significant wave height (H_s) and energy period (T_e) by:

$$J \approx 0.49 H_s^2 T_e \tag{3}$$

As a result, the generic WEC model was allowed to only depend on the following variables: H_s, T_e and $H_s^2 T_e$. The final generic WEC model was formatted as:

$$P_{norm}(t) = A{\cdot}H_s(t) + B{\cdot}H_s^2 T_e(t) + C{\cdot}T_e(t) \tag{4}$$

where A, B, C are fit coefficients, and $P_{norm}(t)$ is the normalized power production. Based on a nonlinear least-squares fitting method, the best performing generic WEC model was determined. Coefficient details are shown in Table 1 under 'Normalized Fit'.

Fig. 10a) provides a visual indication of the performance of the generic WEC model. Overall, the generic model fits the normalized performance matrices of all the WEC architectures very well considering the wide variety of WEC operating principles, reacting bodies, geometric shapes, PTO systems, etc. The model has a power production coefficient of determination (R^2) of 0.849, a sum of squares error (SSE) of 9.87, and a Root-Mean-Square-Error (RMSE) of 0.106 when compared against all the WEC performance data presented in Section 2. The histogram in Fig. 10b, plotting the power production differences between the specific WEC performance datapoints and the generic model, is normally distributed with the greatest uncertainty tails at approximately ± 0.3. The largest deviations (both positive and negative) are in relatively 'large' and low period waves. ($T_e < 7$ s and $H_s > 2$ m waves) where the performance of the differing WEC architectures vary widely. Such conditions occur infrequently, and the impact on final Annual Energy Production (AEP) will be shown to be limited.

While useful, the model developed is limited in application due to the lack of a rated power limit; i.e. the ability for the WEC to unrealistically continue increasing electrical output in highly active/storm conditions. The rated power, or the maximum power that a specific technology can

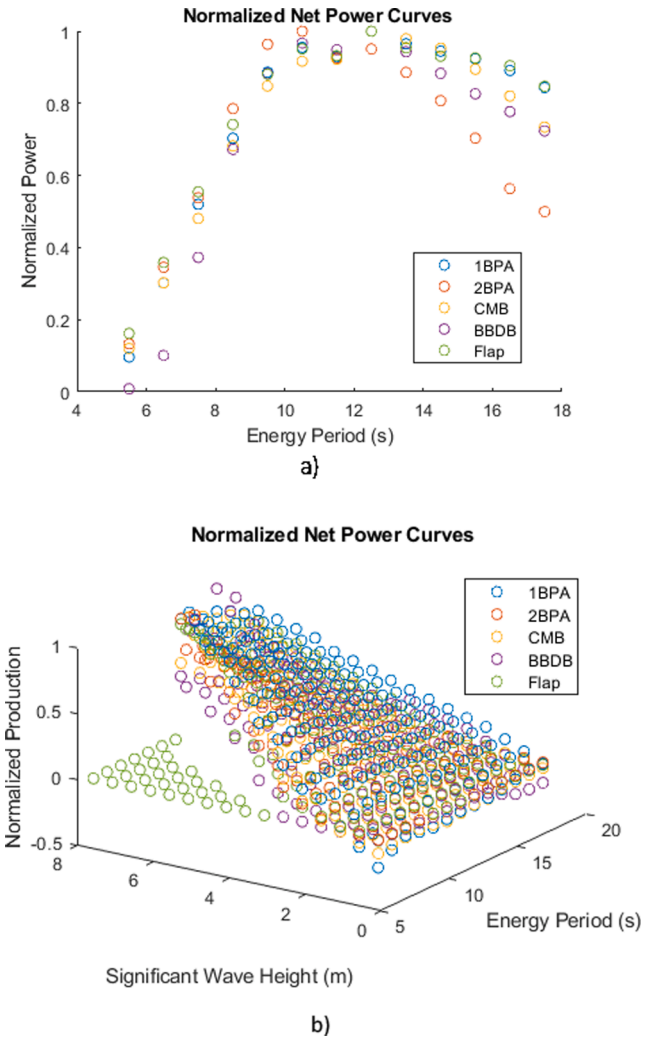

Fig. 9. Normalized WEC Power production in the period domain (a) and in the full sea state domain (b).

Table 1
WEC Power Production Best-Fit Variables and Statistics.

	Equation Coefficients			Uncertainty Statistics		
	A	B	C	R^2	SSE	RMSE
Normalized Fit	0.157	-4.08×10^{-4}	-1.31×10^{-2}	0.849	9.87	0.106
Rated Fit	0.289	-1.11×10^{-3}	-1.69×10^{-2}	0.813	12.0	0.146

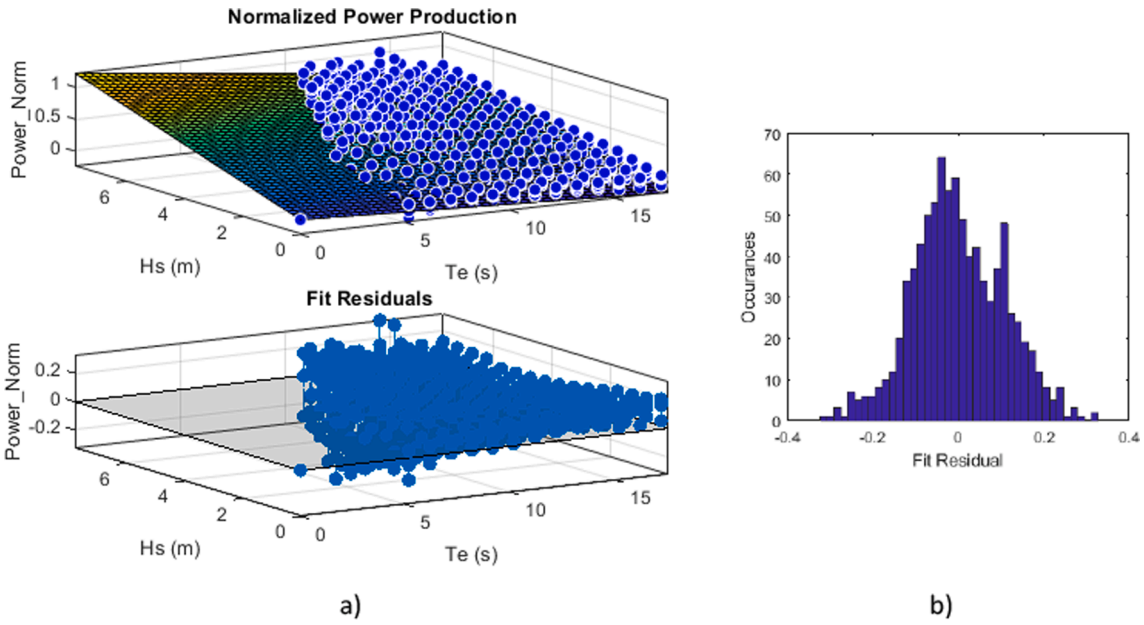

Fig. 10. Normalized Power Production Model Performance against Performance Matrices (a), and Histogram of Fit Residuals (b).

output, is a key requirement for a realistic WEC agnostic representation – this is the focus on the next section.

4.2. Rated power

The rated power represents a realistic maximum production from a WEC. A limit, where independent of increasing gross wave energy transport, the output from the WEC remains constant – as indicated by region three in Fig. 1 for a wind turbine. Unlike other renewables, in which their resource flow can be roughly parameterized by a single variable (e.g. wind speed for wind resources), wave energy is dependent on two variables, and hence identification of a rated power is more complex. Additionally, the rated power is significantly influenced by the generator choice, technology cost, interconnection capacities, system capacity factor and a host of additional parameters.

These are all valuable parameters for WEC designs, but beyond the scope of this research. Following the research objective to develop a generic and tractable representation, based on publicly available data, the generic WEC model was rated based on the 90th percentile of net power production (90th-net). Other power rating methods, such a 90th percentile of the gross wave resource, were investigated with unsatisfactory results.

90th percentile of net WEC power production

The 90th percentile of net WEC power production methodology involves *posteriori* identifying the 90th percentile of the generic WEC production and limiting power output above this value. The methodology can be summarized by the following steps:

1) Following IEC recommendations, the energy production from a WEC is determined by multiplication of sea state conditions (location dependent and parameterized by $H_s$and T_e) and associated production from the non-rated WEC PM.
2) The 90th percentile of the resulting power time-series is identified and used as the rated limit for a specific architecture.
3) This rated limit is transferred back to the WEC PM and is used to normalize all PM values. Examples of resulting rated-limit PM for a OneBPA and a TwoBPA are shown in Fig. 11.
4) A best-fit model is developed to represent the performance of all the WEC architectures, based on their individual rated-limit PMs.

The normalized and rated-limit WEC architecture data cloud and associated best-fit model statistics are shown in Table 1, while visuals in Fig. 12 provide an indication of the performance of the generic performance model. Overall, the model results in a coefficient of determination (R^2) of 0.813 and a limited Root-Mean-Square-Error (RMSE) of 0.146. As shown in the histogram (Fig. 12b), the model uncertainty is slightly positively skewed, with a longer negative tail. As shown with the non-rated model, the largest deviations (both positive and negative)

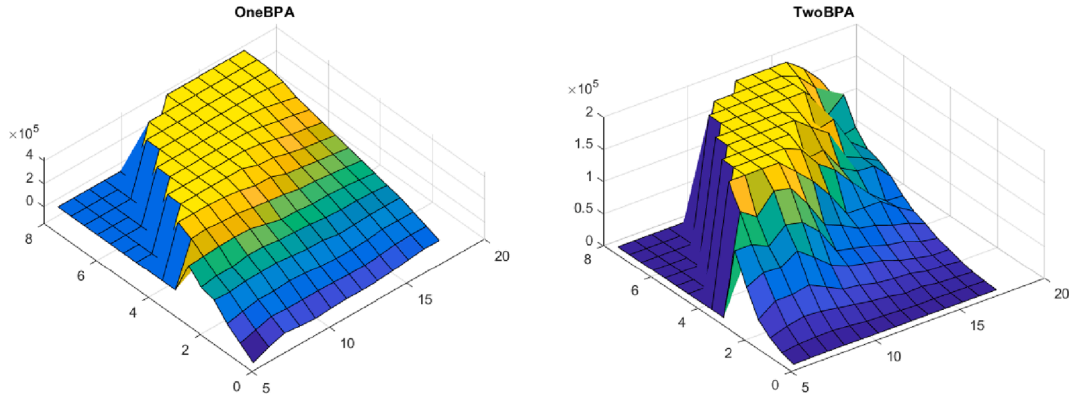

Fig. 11. 90th-Net Rated WEC Performance Matrices.

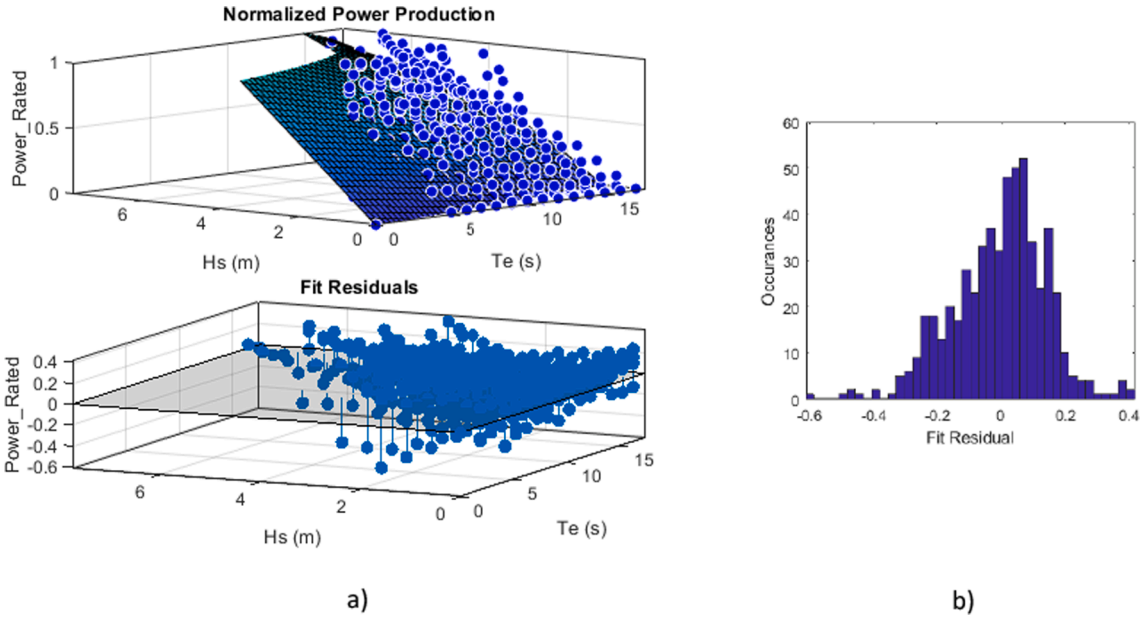

Fig. 12. Normalized Power Production Model Performance against Performance Matrices (a), and Histogram of Fit Residuals (b).

continue to be in relatively 'large' and low period waves (T_e less than 7 s and$H_s > 2$ m waves) where the performance of the differing WEC architectures vary widely.

4.3. WEC agnostic performance model and implementation process

As previously detailed, a normalized generic WEC production model, with cut-in and rated power limits, has been developed. For clarity, this is represented again in Eq. (5), with 95% confidence bounds in Table 2, and shown graphically in Fig. 13.

$$P_{norm}(t) = 0.289 \cdot H_s(t) - 0.00111 \cdot H_s^2(t) T_e(t) - 0.0169 \cdot T_e(t) \quad (5)$$

Fig. 13b) provides a wave-energy converter equivalent of the generic wind turbine model shown in Fig. 1. The 'Rated Power' limit based on the 90th percentile net formulation, and the 'Below Limit', based on the best-fit to excitation forces across the WEC architectures represented. The generic WEC model can also be described by the following mathematical formulation and associated constraints (where P_{norm} represents the normalized rated power):

$$P_{WEC}(t) = P_{norm}(t) * P_{rated} \quad (6)$$

$$P_{norm}(t) = 0.229 \cdot H_s(t) - 0.00111 \cdot H_s^2(t) T_e(t) - 0.0169 \cdot T_e(t) \quad (7)$$

where:

1. $H_s > 0$
2. $T_e > 0$
3. $H_s < \left[0.14 * \left(1.56 T_e^2\right)\right]$ based on the idealized breaking limit for deep water waves.
4. $P_{rated} > 0$ is the rated power capacity of the WEC (in kW).
5. If $P_{norm}(t) < 0, P_{norm}(t) = 0$
6. If $P_{norm}(t) > 1, P_{norm}(t) = 1$

Table 2
95% Confidence Bound Model Coefficients.

	Model Coefficients		
	A	B	C
95% Confidence Bounds	0.275	-1.88×10^{-2}	-1.24×10^{-3}
	0.303	-1.49×10^{-2}	-9.67×10^{-4}

5. Time-series representation

As previously noted, two major knowledge gaps or hurdles are hindering the adoption of WECs into electrical system planning. These are 1) a generic method of representing WEC performance, and 2) a method to up-sample the temporal resolution of traditional and publicly wave buoys and/or numerical wave propagation model outputs. Section 2.1 developed the necessary WEC architecture agnostic representation of power performance, including cut-in and rated capacity limits. This section focussed on the temporal resolution challenge.

While subject to monitoring equipment set-up, wave data from buoys are traditionally recorded and reported at an hourly frequency due to the necessary energy budgets required for higher sampling and data transmission. Numerical wave propagation models (Simulation WAves Nearshore (SWAN)[56], WaveWatch III (WW3) [57], etc.) generally output parameters at 1-hr or 3-hr resolution due to the long length of hindcasts, and the associated computational and storage expense of increased temporal fidelity. The objective of this research is to utilize these status-quo data resources and provide easily applicable and tractable methods to develop WEC higher temporal fidelity power production estimates.

The majority of wave energy, ocean engineering and hydrodynamic analysis utilizes spectral representations of wave conditions and assume linear wave theory applies; i.e. any irregular sea state can be decomposed into a series of regular sinusoidal waves with different amplitudes, wave periods, phases and directions. For more information on linear wave theory and the associated assumptions, readers are referred to [56,58]. Wave spectra are parameterized by H_s and the peak period (T_p), while the marine energy industry additionally utilizes the energy period, T_e. For much of the following analysis, the MATLAB WAFO toolbox is utilized for analysis [59], however, additional details and citations are provided in the remainder of the paper.

Two raw data sets are considered as public-domain and possible input conditions; 1) a time-series of H_s and T_p parameters, or 2) a time-series of wave spectra. For scenario 1), it is necessary to transform the wave parameters to a representative wave spectrum. Unfortunately, these parameters provide insufficient information to accurately recreate the conditions utilized to calculate them, and the research needs to assume a spectral shape in order to proceed. For the North Atlantic and North Sea, the JONSWAP spectrum has been shown to be broadly representative [6]; while for the north-eastern Pacific, a Pierson-

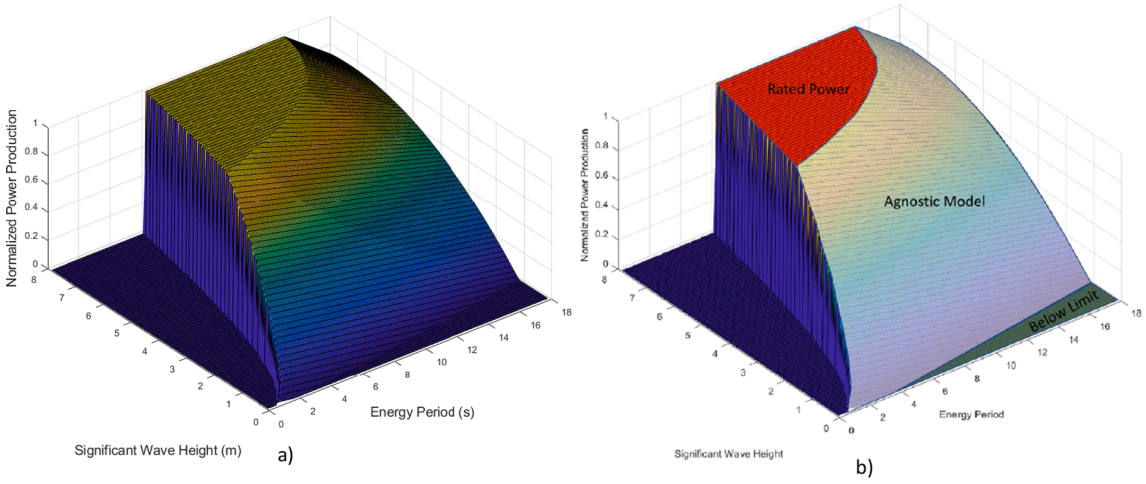

Fig. 13. Generic and normalized WEC performance curve.

Moskowitz (PM) shape has been most representative [22]. The associated PM spectra can be developed following Eq. (8) and Eq. (9) respectively [60]:

$$S_{PM}(f) = 0.3125 H_s^2 T_P \left(\frac{f}{f_p}\right)^{-5} \exp\left[-1.25\left(\frac{f}{f_P}\right)^{-4}\right] \tag{8}$$

$$S_{JONSWAP}(f) = 0.3125 H_s^2 T_P \left(\frac{f}{F_p}\right)^{-5} \exp\left[-1.25\left(\frac{f}{f_P}\right)^{-4}\right](1-0.287\log\gamma)\gamma^{\exp\left[-0.5\left(\frac{\frac{f}{f_P}-1}{\sigma}\right)^2\right]} \tag{9}$$

where f_p is the peak frequency. For the JONSWAP spectra, the following parameter assumptions can be made $\gamma = 3.3$, $\sigma = 0.07$ for frequencies below the peak frequency, and $\sigma = 0.09$ for those above the peak frequency.

The next step involves decomposing the spectra into a water elevation time-series, $\eta(t)$, based on linear superposition of a series of n sinusoidal waves, via the following relationships:

$$\eta(t) = \sum_n a_n \cos(2\pi f_n t + \alpha_n) \tag{10}$$

$$a_n = \sqrt{2 S_{PM}(f_n)\Delta f} \tag{11}$$

$$\alpha_n = \text{rand}(0, 2\pi) \tag{12}$$

where f_n is the wave frequency of the n^{th} wave, a_n is the amplitude of the n^{th} wave, and $\alpha_n$is the associated phase.

The development of sub hour resolved power predictions requires that the wave parameters and the associated spectral be available at this same improved temporal resolution. As a result, the water elevation time series, $\eta(t)$, is now separated into individual data streams of specific time length (i.e. 5/10/15/30 min lengths). These time series are the run through a Fast Fourier Transform (FFT) to develop the associated variance density spectra ($E(f)$), where:

$$E(f) = \lim_{\Delta f \to 0} \frac{1}{\Delta f} E\left\{\frac{1}{2} a_-^2\right\} \tag{13}$$

Subsequently, the associated parameters, based on the spectral moments of $E(f)$ [61], are calculated by:

$$m_n = \sum_i f_i^n S_i \Delta f_i \tag{14}$$

$$H_{m0} = 4\sqrt{m_0} \tag{15}$$

$$T_e = \frac{m_{-1}}{m_0} \tag{16}$$

Eq. (15) provides the zero-moment wave height (H_{m0}), not the significant wave height (H_s). H_{m0} is the correct parameter to utilize for this research. However, the vast majority of the WEC literature refer to H_s when actually defining H_{mo} and, as such, we are maintaining this erroneous title purely to ensure compatibility with the vast majority of published works.

This methodology is visually described in Fig. 14, and a sample of the temporal variability shown in Fig. 15. As shown in Fig. 15, the variability in both H_s and T_e increases considerably as temporal resolution increases. This impact is expected, is representative of true ocean conditions, and will be discussed further in Sections 6 and 7. When conducting this process, it is important to account for aliasing, due to sampling rates, and leakage effects, due to discretely cutting signals under incomplete cycles, when reducing the time-series data. These impacts can be mitigated via ensuring a sufficient sampling resolution (>5Hz) and utilizing band-pass filters to capture relevant wave frequencies [62].

6. Annual energy production and power performance case study results

In order to quantify the annual energy production and power performance, and associated uncertainties, with the proposed

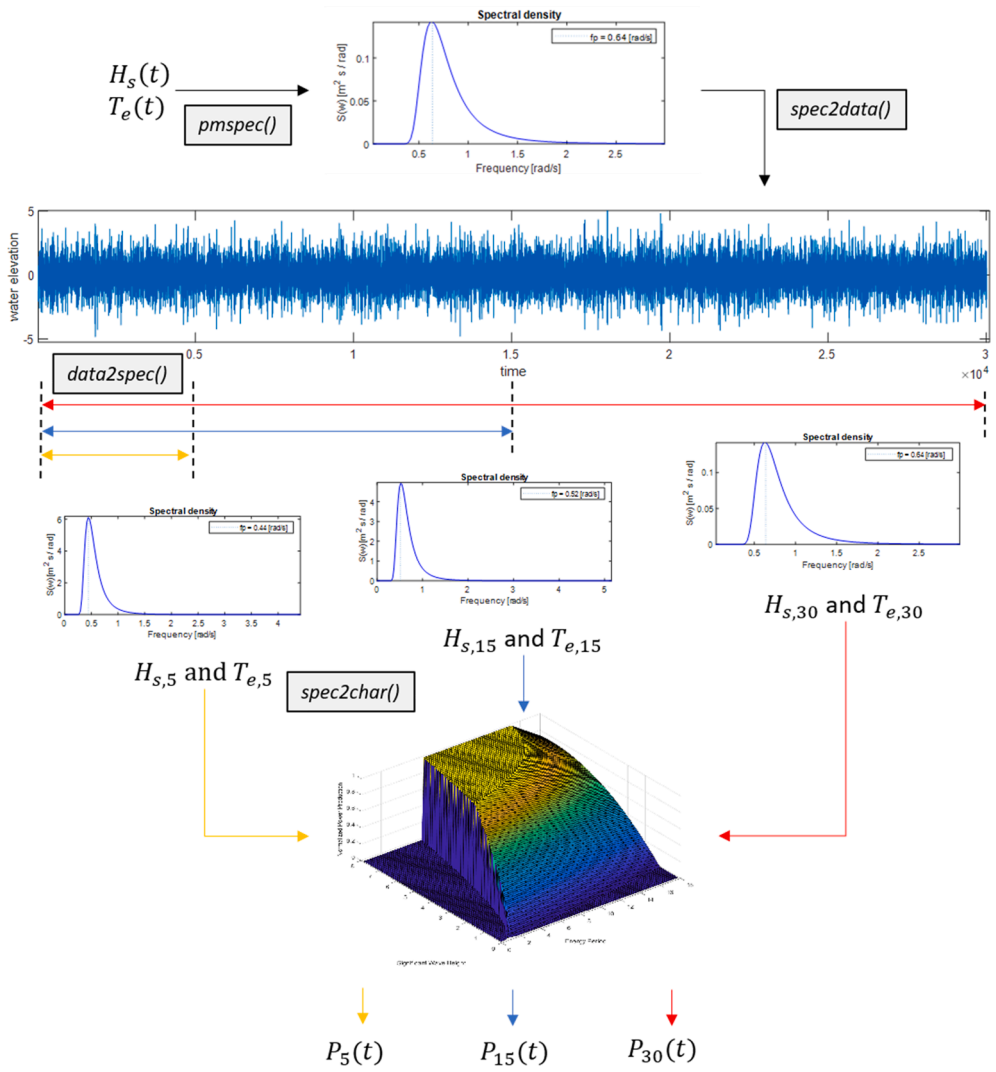

Fig. 14. Flow diagram for the development of time-flexible WEC power predictions. Example functions from the WAFO toolbox are highlighted [59].

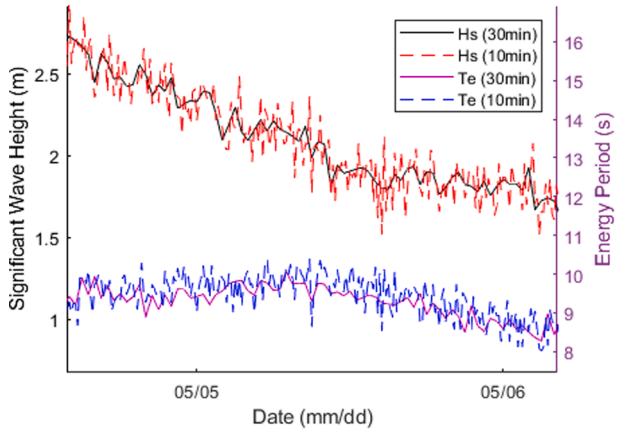

Fig. 15. Temporal variability and impact of up-sampling the significant wave height and energy period during February.

methodologies, a case study for PacWave is conducted. PacWave is a 20 MW grid connected test facility for wave energy conversion technologies under development by Oregon State University off Newport, Oregon, USA.

Utilizing PacWave resource conditions from [63], wave parameters

Table 3
Power and energy production statistics from WEC models and generalized representation.

WEC	Rated Power (kW)	Normalized Power				R^2
		Annual (hr)	Mean	STD	Coef. of Var.	
1BPA	435	4635	0.53	0.26	0.48	0.98
2BPA	190	3584	0.41	0.27	0.67	0.89
CMB	86	3726	0.43	0.34	0.79	0.96
BBDB	209	4057	0.46	0.30	0.64	0.94
FLAP	84	5859	0.67	0.27	0.40	0.87
Generic	TBD	4008	0.46	0.22	0.48	N/A

(H_s and T_e) from 2010 were utilized as an independent dataset to quantify the performance characteristics of the generic WEC model and temporal up-sampling methodology. Following IEC TC-114: 101 [1], the annual energy production, mean production, the standard deviation, coefficient of variation (standard deviation/mean) and the R-Squared between the specific WEC performance and the WEC Agnostic representation are shown in Table 3.

Fig. 16 below plots the normalized power production prediction from the generic WEC model vs the rated WEC power from the high-fidelity ProteusDS numerical model. Note that the horizontal 'lines' result from the discretized nature of the wave parameters (H_s and T_e)

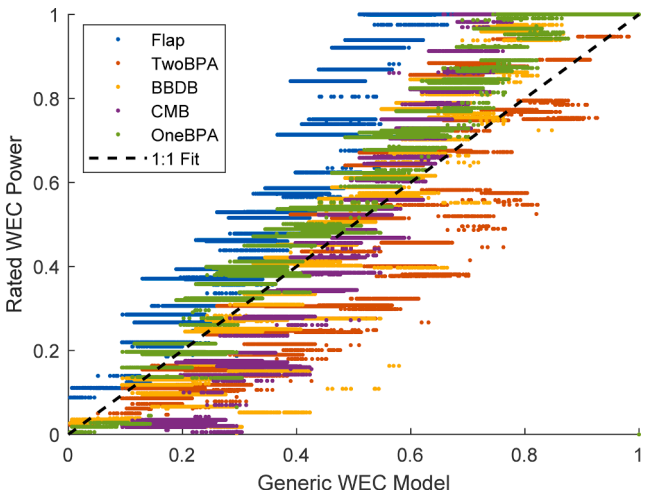

Fig. 16. Generic WEC Model comparison against rated WEC performance.

Table 4
Power and energy production statistics from WEC models and temporal conditions.

Time Resolution	WEC	Normalized Power				
		Annual	Mean	STD	Coef. of Var.	R^2
1BPA	30 min	4635	0.53	0.26	0.48	0.98
	15 min	4598	0.52	0.26	0.49	0.98
	10 min	4572	0.52	0.26	0.49	0.98
	5 min	4526	0.52	0.26	0.50	0.98
2BPA	30 min	3584	0.41	0.27	0.67	0.89
	15 min	3513	0.40	0.27	0.68	0.89
	10 min	3472	0.40	0.27	0.68	0.89
	5 min	3496	0.40	0.27	0.69	0.90
BBDB	30 min	4057	0.46	0.30	0.64	0.94
	15 min	4030	0.46	0.30	0.64	0.95
	10 min	4007	0.46	0.30	0.65	0.95
	5 min	3935	0.45	0.30	0.66	0.94
Generic	30 min	4008	0.46	0.22	0.48	N/A
	15 min	3974	0.45	0.22	0.49	N/A
	10 min	3951	0.45	0.22	0.49	N/A
	5 min	3920	0.45	0.22	0.50	N/A

utilized in the WEC performance matrices (Section 2); based on the ProteusDS modelling.

Table 4 provides an overview of the performance of the differing temporal resolutions on the overall performance of the WEC models, including the generic WEC model. The Flap and CMB buoys were not chosen for further analysis due to their shallow water deployment depth and similarity to the 1BPA respectively.

7. Discussion

Prior to discussing the various assumptions, limitations and implications behind the presented models and results, it is worth revising the objective of this research: The development of an easily implemented, WEC architecture-agnostic, and temporally-flexible model of predicting power production from a wave energy converter, based on publicly available WEC and wave resource datasets.

As detailed in Table 3, and shown in Fig. 16, the generic WEC model provides a reasonably representative prediction of power. However, a number of observations can be made from the presented results. Firstly, the performances of the individual WEC architectures and associated PTO systems vary dramatically across a consistent set of wave conditions – thus, ensuring that any generic model will suffer from significant scatter when compared against any specific WEC. This is apparent in Fig. 16 and, given the specific complexities of each WEC system, maybe unavoidable. For example, the 2BPA is known to have significant parametric roll instabilities, the Flap system relies on wave surge hydrodynamics and is a shallow water only system, the non-linear dynamics of compressed air chambers in the BBDB and staged compression PTO in the CMB create non-trivial hydro-aero-mechanical dynamics which the generic model is unable to replicate. In order replicate and accurately account for these non-linear and more complex dynamics, more sophisticated time-domain models are required and this generic model is not applicable.

Secondly, the generic WEC model overpredicts performance in low production conditions and underestimates in highly active, high performance conditions. This results in both a lower standard deviation and lower coefficient of variation in the generic WEC model. For individual WEC deployments, this uncertainty needs to be considered. For farms of WEC devices, it is feasible that the generic WEC model will provide a realistic representation of farm performance. Finally, it should be noted that all the WEC utilized in this study were focussed on large-scale utility markets and, as such, were of considerable geometric size and associated mass. The impact of this is that the generic WEC model is plausibly only suitable for similar-generation scale uses, and is not suitable for small devices looking at alternate markets (ocean observing, vehicle recharge, etc.) [64]. The application and associated modification of the generic WEC model for different market is recommended for future research.

On temporally flexible methodology, the increased variability of the significant wave height and energy period data, as shown in Fig. 15, is immediately apparent. However, these results are consistent with prior works by Thomson et al. [65] who discovered the significant variability in wave parameters when utilizing shorter FFT windows. They discovered that uniquely short time domain datasets (10 mins) were required to accurately resolve known extreme wave heights. They determined that the spread in wave parameters converges as $1/\sqrt{n}$, where n is the number of measurements per time period. As such, the variance is 10 min wave data is expected to be greater than $30\sqrt{3}$ min data variance – which is immediately apparently in Fig. 15. Positively, the impact of up sampling the wave data is shown to have limited impact on the presented power production and annual energy generation statistics. A slight reduction in annual energy production is apparent with increasing temporal resolution, yet this remains less than 3% for all architectures considered. Almost negligible impacts on the coefficient of variation and the R^2 values are noted due to the up-sampling. Several caveats and assumptions are important when assessing the theoretical and physical accuracy of the temporal up-sampling. Firstly, this methodology assumes that the wave conditions can be represented by a stationary Gaussian process. However, in the ocean and at the shortened time frames (<30 mins) investigated here, the assumption of stationarity is questionable. Ideally, the FFT process would be conducted multiple times over ~30 mins of data, and the associated frequency-dependent variances averaged to create the resulting spectrum. While more robust in creating a repeatable spectrum, this process filters out the natural short-term variability in the ocean parameters. Additionally, as per linear wave theory, one assumes than each wave component acts independently. While a relatively robust assumption for deep water conditions, there are significant wave-wave interactions in steep, developing seas and shallow water conditions. Interested readers are directed to [56] for a detail discussion on non-linear wave interactions.

Finally, it is suggested that the up-sampling methodology should not be ubiquitously applied for very short time periods (less than 5 mins) without *a priori* proving the validity for a specific location and architecture. It is expected that, whilst the representation of the sea conditions is statistically sound, the application of a WEC power performance values (generated as a mean of a 20-mins numerical simulation) will under-predict important fluctuations in power and may not provide a reliable estimate for all components. However, as detailed in the motivation for this research, the objective was to develop a reasonable technology-agnostic and time-flexible representation of WEC power

production, based on publicly available data. For highly resolved time-series, it is suggest that that the technical specifications developed under the International Electrotechnical Commission TC-114 committee would be most suitable [66].

8. Conclusions

The growth of the wave energy sector is contingent on the ability for stakeholders, particularly electrical utilities, to rapidly predict the production from wave energy converters (WECs). Current methodologies require extensive knowledge of metocean conditions, *a priori* determination of WEC architecture, and highly-specific physical and numerical tools. Additionally, the lack of a consistent robust method up-sample the hourly temporal resolution of traditional wave buoys and/or numerical wave propagation models limits the implementation of wave energy technologies in Integrated Resource Planning (IRP) by utilities. These two knowledge gaps create a significant barrier for broad adoption of wave energy. This novel research provides an overview of a consistent and coherent waves-to-wire method to quantify WEC performance data, across wide variety of technology architectures, to develop an empirically driven and easily applicable generic model of WEC performance.

The comparison of the generic WEC performance model against the OneBPA, TwoBPA, CMB, Flap and BBDB WEC architectures ultimately shows an average co-efficient of determination (R^2) of 0.93 (based on hourly power production), and less than 9% variation in annual energy production. The generic WEC model is shown to slightly over-estimate performance in low energy sea-states and over-estimate in high energy sea-states. Given the wide variety of WEC architectures, PTO systems, non-linear system dynamics, and the 'tractable to non-experts' objective, the performance of the model is significant.

The temporal up-sampling methodology is shown to increase the temporal variability of bulk wave parameters, as previously quantified against measurements at the same site by Thomson et al. [65], yet often neglected. While the short-term variability in significant wave height, energy period, and WEC production all increase, the annual mean and total energy production are not altered in any significant manner thus providing additional confidence in the prescribed method.

In conclusion, the newly developed generic WEC model and time-flexible representation of conditions replicates similar successful generic performance models from the wind and solar industries to provide an easily applicable method to predict performance; based on publicly available data. This research overcomes two known knowledge gaps which have historically created a significant barrier for broad planning and adoption of wave energy for marine energy conversion.

CRediT authorship contribution statement

Bryson Robertson: Conceptualization, Resources, Investigation, Funding acquisition. **Helen Bailey:** Methodology, Software, Data curation. **Matthew Leary:** Methodology, Software, Data curation. **Bradley Buckham:** Conceptualization, Investigation, Funding acquisition.

Declaration of Competing Interest

The authors declare that they have no known competing financial interests or personal relationships that could have appeared to influence the work reported in this paper.

References

[1] International Electrotechnical Commission. IEC TS 62600-101:2015; 2015.
[2] Lenee-Bluhm P, Paasch R, Özkan-Haller HT. Characterizing the wave energy resource of the US Pacific Northwest. Renew Energy 2011;36:2106–19. https://doi.org/10.1016/j.renene.2011.01.016.
[3] Robertson B, Bailey H, Clancy D, Ortiz J, Buckham B. Influence of wave resource assessment methodology on wave energy production estimates. Renew Energy 2016;86:1145–60. https://doi.org/10.1016/j.renene.2015.09.020.
[4] López-Ruiz A, Bergillos RJ, Raffo-Caballero JM, Ortega-Sánchez M. Towards an optimum design of wave energy converter arrays through an integrated approach of life cycle performance and operational capacity. Appl Energy 2018;209:20–32. https://doi.org/10.1016/j.apenergy.2017.10.062.
[5] Robertson B, Hiles C, Luzko E, Buckham B. Quantifying Wave Power and Wave Energy Converter Array Production Potential. Int J Mar Energy 2015:1. https://doi.org/10.1016/j.ijome.2015.10.001.
[6] Guedes Soares C, Bento AR, Gonçalves M, Silva D, Martinho P. Numerical evaluation of the wave energy resource along the Atlantic European coast. Comput Geosci 2014;71:37–49. https://doi.org/10.1016/j.cageo.2014.03.008.
[7] Pilar P, Soares CG, Carretero JC. 44-year wave hindcast for the North East Atlantic European coast. Coast Eng 2008;55:861–71.
[8] Neill SP, Hashemi MR. Wave power variability over the northwest European shelf seas. Appl Energy 2013;106:31–46. https://doi.org/10.1016/j.apenergy.2013.01.026.
[9] Sierra JP, Martín C, Mösso C, Mestres M, Jebbad R. Wave energy potential along the Atlantic coast of Morocco. Renew Energy 2016;96:20–32. https://doi.org/10.1016/j.renene.2016.04.071.
[10] Alonso R, Solari S, Teixeira L. Wave energy resource assessment in Uruguay. Energy 2015;93:683–96. https://doi.org/10.1016/j.energy.2015.08.114.
[11] Hemer MA, Griffin DA. The wave energy resource along Australia's Southern margin. J Renew Sustain Energy 2010:2. https://doi.org/10.1063/1.3464753.
[12] Behrens S, Hayward J, Hemer M, Osman P. Assessing the wave energy converter potential for Australian coastal regions. Renew Energy 2012;43:210–7. https://doi.org/10.1016/j.renene.2011.11.031.
[13] Lavidas G, Venugopal V. Prospects and applicability of wave energy for South Africa. Int J Sustain Energy 2018;37:230–48. https://doi.org/10.1080/14786451.2016.1254216.
[14] Robertson BRD, Hiles CE, Buckham BJ. Characterizing the near shore wave energy resource on the west coast of Vancouver Island, Canada. Renew Energy 2014:71. https://doi.org/10.1016/j.renene.2014.06.006.
[15] Robertson B, Bailey H, Clancy D, Ortiz J, Buckham B. Influence of wave resource assessment methodology on wave energy production estimates. Renew Energy 2016:86. https://doi.org/10.1016/j.renene.2015.09.020.
[16] BCHydro. Integrated Resource Plan; 2013.
[17] PG&E. Intergrated Resource Plan 2020; 2020.
[18] Kusiak A, Verma A. Monitoring wind farms with performance curves. IEEE Trans Sustain Energy 2013;4:192–9. https://doi.org/10.1109/TSTE.2012.2212470.
[19] Bosma B, Brekken TKA, Özkan-Haller HT, Yim SC. Wave energy converter modeling in the time domain: A design guide. 2013 1st IEEE Conf Technol Sustain SusTech 2013 2013:103–8. https://doi.org/10.1109/SusTech.2013.6617305.
[20] Illesinghe SJ, Manasseh R, Dargaville R, Ooi A. Idealized design parameters of Wave Energy Converters in a range of ocean wave climates. Int J Mar Energy 2017;19:55–69. https://doi.org/10.1016/j.ijome.2017.03.003.
[21] de Andres A, Guanche R, Vidal C, Losada IJ. Adaptability of a generic wave energy converter to different climate conditions. Renew Energy 2015;78:322–33. https://doi.org/10.1016/j.renene.2015.01.020.
[22] Robertson B, Bailey H, Buckham B. Resource assessment parameterization impact on wave energy converter power production and mooring loads. Appl Energy 2019;244:1–15. https://doi.org/10.1016/j.apenergy.2019.03.208.
[23] Babarit A. A database of capture width ratio of wave energy converters. Renew Energy 2015;80:610–28. https://doi.org/10.1016/j.renene.2015.02.049.
[24] Rusu L, Onea F. The performance of some state-of-the-art wave energy converters in locations with the worldwide highest wave power. Renew Sustain Energy Rev 2017;75:1348–62. https://doi.org/10.1016/j.rser.2016.11.123.
[25] Parkinson SC, Dragoon K, Reikard G, García-Medina G, Özkan-Haller HT, Brekken TKA. Integrating ocean wave energy at large-scales: A study of the US Pacific Northwest. Renew Energy 2015;76:551–9. https://doi.org/10.1016/j.renene.2014.11.038.
[26] Robertson B, Hiles C, Luczko E, Buckham B. Quantifying wave power and wave energy converter array production potential. Int J Mar Energy 2016:14. https://doi.org/10.1016/j.ijome.2015.10.001.
[27] Babarit A, Hals J, Muliawan MJ, Kurniawan A, Moan T, Krokstad J. Numerical benchmarking study of a selection of wave energy converters. Renew Energy 2012;41:44–63.
[28] Xu X, Robertson B, Buckham B. A techno-economic approach to wave energy resource assessment and development site identification. Appl Energy 2020;260:114317. https://doi.org/10.1016/j.apenergy.2019.114317.
[29] Blanco M, Moreno-Torres P, Lafoz M, Ramírez D. Design parameter analysis of point absorber WEC via an evolutionary-algorithm-based dimensioning tool. vol. 8; 2015. https://doi.org/10.3390/en81011203.
[30] Bailey H, Robertson B, Buckham BJ. Optimizing WECs for Canadian waters. Int. Conf. Ocean Energy, ICOE 2014.
[31] Beatty SJ, Hall M, Buckham BJ, Wild P, Bocking B. Experimental and numerical comparisons of self-reacting point absorber wave energy converters in regular waves. Ocean Eng 2015:104. https://doi.org/10.1016/j.oceaneng.2015.05.027.
[32] Harris RE, Johanning L, Wolfram J. Mooring systems for wave energy converters: A review of design issues and choices. 3rd Int Conf Mar Renew Energy 2004:1–10.
[33] Weinstein A, Fredrikson G, Parks MJ, Nielsen K. AquaBuOY - The offshore wave energy converter numerical modeling and optimization. Ocean '04 - MTS/IEEE Techno-Ocean '04 Bridg across Ocean - Conf Proc 2004;4:1854–9. https://doi.org/10.1109/oceans.2004.1406425.

[34] Brown A, Thomson J, Rusch C. Hydrodynamic Coefficients of Heave Plates, with Application to Wave Energy Conversion. IEEE J Ocean Eng 2018;43:983–96. https://doi.org/10.1109/JOE.2017.2762258.

[35] Beatty SJ, Bocking B, Bubbar K, Buckham BJ, Wild P, Data M, et al. Experimental and numerical comparisons of self-reacting point absorber wave energy converters in irregular waves. Ocean Eng 2019;173:716–31. https://doi.org/10.1016/j.oceaneng.2019.01.034.

[36] Beatty S, Ferri F, Bocking B, Kofoed JP, Buckham B. Power take-off simulation for scale model testing of wave energy converters. Energies 2017:10. https://doi.org/10.3390/en10070973.

[37] Bailey H, Robertson B, Buckham B. Variability and stochastic simulation of power from wave energy converter arrays. Renew Energy 2018:115. https://doi.org/10.1016/j.renene.2017.08.052.

[38] Yu YH, Hallett K, Li Y, Hotimsky C. Design and analysis for a floating oscillating surge wave energy converter. Proc Int Conf Offshore Mech Arct Eng - OMAE 2014; 9B:1–10. https://doi.org/10.1115/OMAE2014-24511.

[39] Cameron L, Doherty R, Henry A, Doherty K, Van't Hoff J, Kaye D, et al. Design of the next generation of the Oyster wave energy converter. 3rd Int Conf Ocean Energy 2010:1–12.

[40] Lucas J, Livingstone M, Vuorinen M, Cruz J. Development of a wave energy converter (WEC) design tool – application to the WaveRoller WEC including validation of numerical estimates. Proc 4th Int Conf Ocean Energy 2012.

[41] Ramudu E. Ocean wave energy-driven desalination systems for off-grid coastal communities in developing countries. Proc - 2011 IEEE Glob Humanit Technol Conf GHTC 2011 2011:287–9. https://doi.org/10.1109/GHTC.2011.38.

[42] Ruehl K, Forbush DD, Yu YH, Tom N. Experimental and numerical comparisons of a dual-flap floating oscillating surge wave energy converter in regular waves. Ocean Eng 2020;196:106575. https://doi.org/10.1016/j.oceaneng.2019.106575.

[43] Thacher E, Bailey H, Robertson B, Beatty S, Goldsworthy J, Crawford C, et al. Development of control strategies for interconnected pneumatic wave energy converters. Proc. Int. Conf. Offshore Mech. Arct. Eng. - OMAE, vol. 10, 2017. https://doi.org/10.1115/OMAE2017-61537.

[44] Bull D, Smith C, Jenne DS, Jacob P, Copping A, Willits S, et al. Reference Model 6 (RM6): Oscillating Wave Energy Converter 2014;6.

[45] Folley M, Babarit A, Child BFM, Forehand D, O'Boyle L, Silverthorne K, et al. A Review of Numerical Modelling of Wave Energy Converter Arrays. ASME 2012 31st Int. Conf. Ocean. Offshore Arct. Eng., Rio de Janeiro: 2012, p. 1–12.

[46] Bailey H, Robertson B, Ortiz J, Buckham B, Wecs AT. Stochastic Methods to Predict WEC Array Power for Grid Integration. Proceeding from Eur. Wave Tidal Energy Conf. (EWTEC), Nantes, France: n.d.

[47] Bailey H, Ortiz J, Robertson B, Buckham B, Nicoll R. A Methodology for Wave-To-Wire WEC Simulations. Mar Renew Energy Technol Symp 2014:1–15.

[48] McNeel R. Rhinoceros User Guide. 2020 n.d. http://docs.mcneel.com/rhino/6/usersguide/en-us/index.htm.

[49] Tobergte DR, Curtis S. WAMIT User Manual. vol. 53; 2013. https://doi.org/10.1017/CBO9781107415324.004.

[50] Andersson E. Application of the open source code Nemoh for modelling of added mass and damping in ship motion simulations; 2018.

[51] McTaggart KA. ShipMo3D Version 3.0 User Manual for Computing Ship Motions in the Time and 2012.

[52] Newman JN. Marine Hydrodynamics. The MIT Press; 1977.

[53] DSA L. Dynamic Systems Analysis Ltd ProteusDS Manual; 2013.

[54] Buckham BJ, Nahon M. Formulation and validation of a lumped mass model for low-tension ROV tethers. Int J Offshore Polar Eng 2001;11.

[55] Goda Y. Random Seas and Design of Maritime Structures. Adv Ser Ocean Eng World Sci 2009;33:708.

[56] Holthuijsen LH. Waves in Oceanic and Coastal Waters. Cambridge University Press; 2007.

[57] NCEP UNC for EP. NOAA WaveWatch III 2012. http://polar.ncep.noaa.gov/waves/implementations.shtml? [accessed April 8, 2016].

[58] Dean RG, Dalrymple RA. Water Wave Mechanics for Engineers and Scientists, vol. 2. Singapore: World Scientific Publishing; 1991.

[59] Group W. WAFO–A Matlab toolbox for analysis of random waves and loads. Sweden: Lund Inst Technol Lund; 2000.

[60] Ts IEC. IEC TS 61400-3-2 TECHNICAL; 2020.

[61] International Electrotechnical Commission T C 114. IEC TS 62600-101 Technicial Specification - Part 101: Wave energy resource assessment and characterization; 2015.

[62] Brown A, Thomson J, Ellenson A, Rollano FT, Ozkan-Haller HT, Haller MC. Kinematics and Statistics of Breaking Waves Observed Using SWIFT Buoys. IEEE J Ocean Eng 2019;44:1011–23. https://doi.org/10.1109/JOE.2018.2868335.

[63] Dunkle G, Robertson B, Garcia-Medina G, Yang Z. PacWave Wave Resource Assessment; 2020.

[64] US DOE Water Power Technologies Office. Powering the Blue Economy: Exploring Opportunities for Marine Renewable Energy in Maritime Markets | Department of Energy 2019. https://www.energy.gov/eere/water/powering-blue-economy-exploring-opportunities-marine-renewable-energy-maritime-markets [accessed June 24, 2019].

[65] Thomson J, Brown A, Ellenson A, Haller M. Extreme Conditions at Wave Energy Sites n.d.:8–11.

[66] IEC. TC114: Marine energy - wave, tidal and other water current converters. - Part 101: Wave energy resource assessment and characterization. TS Ed.1: International Electrotechnical Commission; 2015.